Water SA 51(3) 243–255 / Jul 2025
https://doi.org/10.17159/wsa/2025.v51.i3.4158

Critical incipient failure conditions for angular riprap on steep trapezoidal channels using the movability number

M Appolus[1], A Bosman[1] and GR Basson[2]

[1]*Civil Engineering Department, Water Division, Stellenbosch University, Stellenbosch, South Africa*
[2]*Emeritus Professor, Department of Civil Engineering, Stellenbosch University, Stellenbosch, South Africa*

A 1:15 scale physical hydraulic model was designed and constructed to investigate the incipient failure conditions of large angular riprap. A total of 32 tests were performed on angular riprap dumped on steep bed slopes of 0.333 to 0.5, and against a steep side-bank slope of 0.4 in a wide trapezoidal channel. The critical movability number value defining the critical incipient failure conditions of angular riprap on steep bed slopes and steep side-bank slopes was determined to be 0.12 and 0.227, respectively. Based on the HEC-RAS 1-dimensional (1-D) steady-state flow analysis, it was identified that HEC-RAS overestimates the critical incipient failure movability number of the steep bed and steep side-bank riprap by a critical factor of 1.91 and 1.35, respectively. The applicability of the study's findings is limited to prototype riprap D_{50} sizes of 0.57 m to 1.125 m, and a trapezoidal canal bottom-width to D_{50} ratio of 16:31 (W_{base}: D_{50}).

CORRESPONDENCE
A Bosman

EMAIL
abosman2@sun.ac.za

DATES
Received: 15 July 2024
Accepted: 4 June 2025

KEYWORDS
incipient failure
incipient motion
riprap
steep slopes
movability number

INTRODUCTION

Steep canal beds and riverbanks are highly susceptible to erosion from turbulent flow. Riprap protection is a widely endorsed method for controlling river erosion due to its aesthetic appearance, minimal environmental impact, cost-effective solution (especially when rocks are locally available), ease of construction and maintenance, and durable and reusable properties (Langmaak and Basson, 2015; California Division of Highways, 1970; Committee of State Road Authorities, 1994).

The general hydrodynamic behaviour of riprap has been the subject of numerous studies and is fairly well understood. The determination of the preferred rock gradation (Stevens et al., 1979), riprap thickness (Frizell et al,. 1998), length of protection (De Almeida and Martín-Vide, 2009), the most stable rock shape and angle of repose of riprap (Froehlich, 2011) have been explored in previous years. Recent riprap research has been based on the testing of stable sizes of riprap rock on canal beds with different longitudinal slopes, i.e., in the flow direction. These riprap studies have been based mainly on flat and gentle bed slopes armoured with round shaped stones. However, the sizing of angular riprap in steep canal beds and steep side banks has not been thoroughly investigated. This gap in knowledge motivated a research study at Stellenbosch University, South Africa, to examine the stability of angular riprap on steep longitudinal riverbed slopes and steep trapezoidal cross-sectional slopes of riverbanks.

Previous studies, such as Langmaak and Basson (2015), have investigated the stability of riprap on steep longitudinal bed slopes. However, these studies only examined the incipient motion of riprap on the steep bed area. Langmaak and Basson (2015) showed that the movability number (MN)–based approach can be effectively used to analyse the incipient motion of large riprap dumped on steep bed channels. The present study expands on this work by analysing the stability of purely angular riprap on wide trapezoidal cross-sectional channels with hydraulically steep longitudinal bed slopes and steep side-bank slopes, using Liu's (1957) stream power–based theory, known as the MN approach or methodology.

The main objectives of this study were to determine the stable hydraulic conditions of riprap on steep bed and side-bank slopes of wide trapezoidal channels, and to recommend a method for specifying stable riprap sizes for these conditions.

THEORETICAL FRAMEWORK

Incipient motion in terms of stream power

The stream power approach to studying incipient motion has emerged as a preferred theoretical approach, offering advantages over shear stress–based and velocity-based incipient motion approaches (Yang and Stall, 1974; Rooseboom and Mulke, 1982; Yang, 1984; Ferguson, 2005). According to the stream power law, the total input stream power equals the total applied stream power. This principle was mathematically defined by Rooseboom (1974) as:

$$\int_{y_0}^{D} \rho_w g S_0 V \, dy = \int_{y_0}^{D} \tau_0 \frac{du}{dy} dy \quad (1)$$

where y_0 is the ordinate where the velocity is theoretically equal to zero, y is the vertical distance above the bed level, ρ_w is the water density, g is the gravitational acceleration, S_0 is the canal bed slope, V is the flow velocity at distance y above the bed, τ_0 is the shear stress, and $\frac{du}{dy}$ is the velocity gradient.

In Eq. 1, the left-hand side represents the available stream power, while the right-hand side represents the applied stream power. This relationship is illustrated in Fig. 1, where the area under the available stream power curve (blue) equals the orange area under the applied stream power curve (orange).

The stream power dissipation curve in Fig. 1 illustrates a decreasing exponential trend from top to bottom, indicating a decrease in stream power. This decline is attributed to the shear stress, which is theoretically zero at the surface and a maximum at the bottom of the bed.

Rooseboom (1992) suggested that the treatment of stream power differs between laminar and turbulent flow regimes, particularly regarding the velocity gradient $\left(\frac{du}{dy}\right)$ in Eq. 1. Langmaak and Basson (2015) describe the stream power transfer in the laminar flow as occurring from fast to slow-moving layers of water. In turbulent flow regions, the stream power is transferred from fast-moving eddies through collisions with the slower moving water pockets, decelerating the faster moving eddies and accelerating the slower water packets.

Linking stream power to the movability number

The literature suggests that incipient motion can be understood through theoretical frameworks involving shear stress, velocity and stream power (Shield, 1936; Maynord et al., 1989; Yang, 1984). Armitage (2002) argues that these three incipient motion frameworks are interconnected, with the MN derived from the stream power theory (Rooseboom, 1992). Liu (1957) defined the MN as the ratio of the shear velocity (u^*) to the settling velocity (v_{ss}) as follows:

$$\mathrm{MN} = \frac{u^*}{v_{ss}} \tag{2}$$

with the shear velocity (u^*) linked to the bed shear stress (τ_0) defined by Armitage (2002) as:

$$u^* = \sqrt{\frac{\tau_0}{\rho_w}}. \tag{3}$$

Based on Eqs 2 and 3, Armitage (2002) concludes that the MN is proportional to the square root of the bed shear stress.

According to Langmaak and Basson (2015), Rooseboom (1992) demonstrated that stream power initiates particle movement when the power needed to suspend a particle exceeds the power required to keep the particle in its static position:

$$\frac{(\rho_r - \rho_w)D_{50}}{\rho_w S_o D_w} \propto \frac{\sqrt{gD_w S_o}}{v_{ss}}, \tag{4}$$

with ρ_r and ρ_w the density of rock and water respectively, S_o the longitudinal bed slope, D_w the flow depth, and v_{ss} the settling velocity of the rock block.

In the turbulent flow regime, Eq. 4 is simplified to (Langmaak and Basson, 2015):

$$\frac{\sqrt{gD_w S_o}}{v_{ss}} = \text{constant} \tag{5}$$

This constant is known as the MN, which is an empirical constant that depends on the settling velocity of the pertinent particle (v_{ss}), the bed slope (S_o), and the average flow depth (D_w). Moreover, since $\sqrt{gD_w S_o} = u^*$, Eq. 5 can be written as Eq. 2.

Rooseboom (1992) analysed Grass (1970) and Yang's (1973) data and found that the MN for turbulent flow is $\frac{u_*}{v_{ss}} = 0.12$ using Eq. 5, whereas Armitage (2002) determined the critical MN to be 0.17. These two studies were based on different methods, explaining the different findings. Langmaak and Basson (2015) report a critical MN value of 0.18 for large riprap on steep bed slopes, incorporating a steep bed correction factor (k_β) to account for the influence of the steep bed. Therefore, the MN equation applicable for the specific study was as follows:

$$\mathrm{MN} = \sqrt{k_\beta}\,\frac{\sqrt{gD_w S_o}}{v_{ss}} \tag{6}$$

with the correction factor defined as (Armitage, 2002):

$$k_\beta = \frac{\sin(\varphi_r - \beta)}{(\sin\varphi_r)} \tag{7}$$

where: φ_r is the riprap rock angle of repose, and β is the steep bed angle. Additionally, Armitage (2002) defined the side bank steep correction as follows (also in Henderson, 1966):

$$k_\alpha = \cos\alpha\sqrt{1 - \frac{\tan^2\alpha}{\tan^2\varphi_r}} \tag{8}$$

where α is the side bank angle. Considering the two steep slope correction factors, the complete MN equation accounting for both steep bed slopes and steep side slopes may be written as follows (Armitage, 2002):

$$\mathrm{MN} = \sqrt{k_\beta k_\alpha}\,\frac{\sqrt{gD_w S_o}}{v_{ss}}. \tag{9}$$

The literature supports using the MN to study incipient motion, building on established theoretical foundations (Rooseboom, 1992). Langmaak and Basson (2015) demonstrate the effectiveness of using the MN in studying large riprap on steep slopes with the appropriate correction factors recommended by Armitage (2002).

PHYSICAL HYDRAULIC MODEL STUDY

The stability of angular riprap on wide trapezoidal cross-sectional channels with hydraulically steep longitudinal bed and side-bank slopes was investigated using physical modelling. An undistorted physical hydraulic model scale of 1:15 was selected to limit scaling effects.

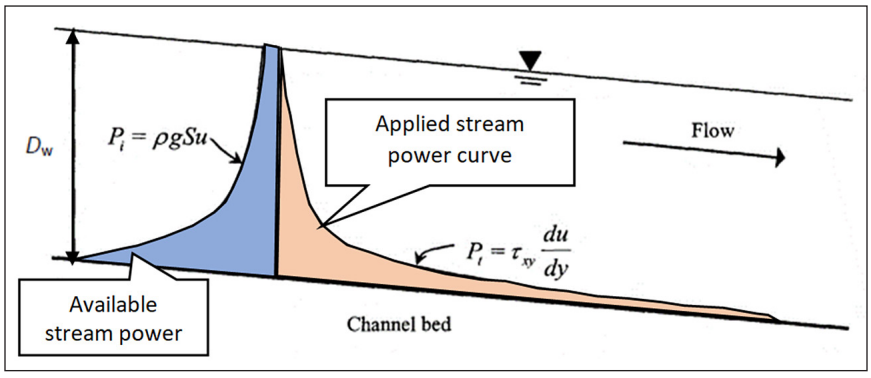

Figure 1. Distribution of available and applied stream power in an arbitrary reach (Rooseboom, 1992)

The physical model, shown in Fig. 2, consisted of graded D_{50} rock sizes of 0.038 m and 0.075 m, equivalent to D_{50} of 0.57 m and 1.125 m at prototype scale, respectively. These riprap sizes were dumped on three steep longitudinal bed slopes (0.333, 0.4 and 0.5) and one steep side-bank slope (0.4), representing typical conditions in river revetment designs.

The test setups comprised of three main testing series:

1. **Test Series 1** examined the incipient motion failure conditions of the D_{50} = 0.038 m angular riprap rock on the 0.333, 0.4 and 0.5 steep bed slopes and 0.4 steep side-bank slope.
2. **Test Series 2** investigated the incipient motion failure conditions of the D_{50} = 0.075 m angular riprap rock on the same bed and side-bank slopes as test series one.
3. **Test Series 3** focused on the incipient motion failure conditions of the D_{50} = 0.075 m angular riprap rock on the 0.333 and 0.5 steep bed slopes and 0.4 steep side-bank slope. Unlike in Series 1 and 2, the riprap on the bed area was fixed using an adhesive to prevent movement, allowing the investigation of the incipient failure conditions of riprap on the side bank. This approach was informed by findings from Test Series 1 and 2, where riprap on the bed failed before any movement was observed on the side bank, with no significant water encroachment.

Table 1 summarises the hydraulic test schedule for the tests executed.

The laboratory setup, illustrated in Fig. 3, involved conveying flow into the canal through the hydraulic laboratory's pipelines, which were fed by water pumped up from an underground water storage facility and directed into the testing flume. The water passed through the flowmeter before entering the channel's stilling basin. A control valve regulated the flow into the stilling basin, where the water–floor impact induced the formation of air bubbles, turbulent eddies and vortexes. To mitigate upstream surface water waves, flow straighteners were installed upstream of the stilling basin area. No gate was installed at the downstream end of the model, allowing water to flow freely into the laboratory's drainage system downstream as illustrated by Fig. 3.

Hydraulic model design and construction

The main physical model design parameters included the model shape, hydraulic transitions due to change in cross-section, bed and side-bank slopes, and the arrestor length (L_{arr}). The shape of the model adhered to a trapezoidal cross-section, with steep bed slopes of 0.333 to 0.5 and side bank of 0.4, aligning with the study's objectives.

The transitional cross-sections were designed to minimize energy losses, with tapers of 1:4 in the upstream and downstream transitional flow areas (see Fig. 4 in conjunction with Fig. 2). The arrestor length (L_{arr}) was determined based on recommendations from previous studies (De Almeida and Martín-Vide, 2009), with $L_{arr} \geq 16\ D_{50}$. Due to laboratory spatial limitations, a 1 m L_{arr} was used, which was sufficient for the full development of flow in all the tests.

Figure 5 illustrates the testing zone, with a bed slope of 0.5 where the slope was changed based on the test series (i.e. changed from 0.333 to 0.4 and 0.5). The steep side-bank slope of 0.4 remained constant for all the tests.

The foundation of the physical model was constructed using bricks and concrete blocks inside a 1.2 m wide and 1.6 m deep flume. Smaller aggregate stones, approximately 5–10 mm D_{50} size, were used to fill in the voids within the bricks and blocks, and to achieve a level surface. Figure 6 illustrates the completed foundation level. To ensure water tightness, cross-sectional wooden boards were installed in the foundation, and plastic sheeting was placed over the complete foundation level (refer to Fig. 5). A geotextile Bidim material was used as a filter layer.

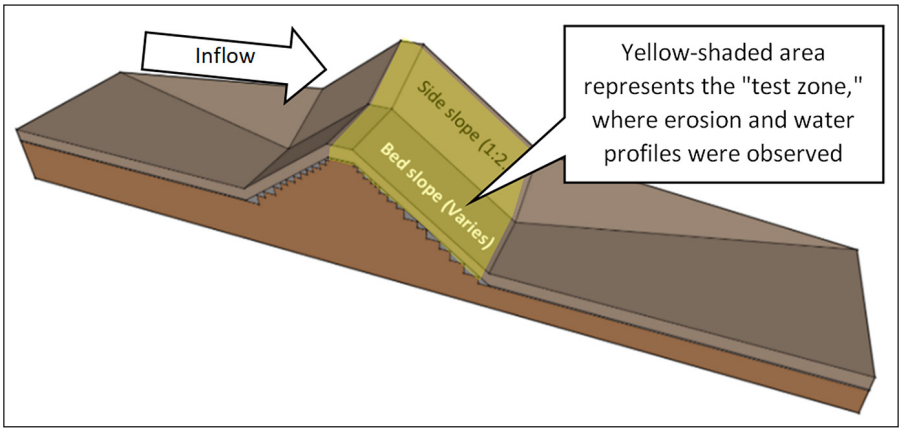

Figure 2. Oblique view of the hydraulic testing zone

Table 1. Testing schedule of the laboratory hydraulic models

Test series	Test No.	D_{50} Size (m)	Bed slope	Movable bed	Side bank slope	Movable bank	Total no. of tests
1	1–3	0.038	1:2	Yes	1:2.5	Yes	7
	6		1:2.5	Yes	1:2.5	Yes	
	7–9		1:3	Yes	1:2.5	Yes	
2	1–5	0.075	1:2	Yes	1:2.5	Yes	15
	6–10		1:2.5	Yes	1:2.5	Yes	
	11–15		1:3	Yes	1:2.5	Yes	
3	1–5	0.075	1:2	No	1:2.5	Yes	10
	6–10		1:3	No	1:2.5	Yes	

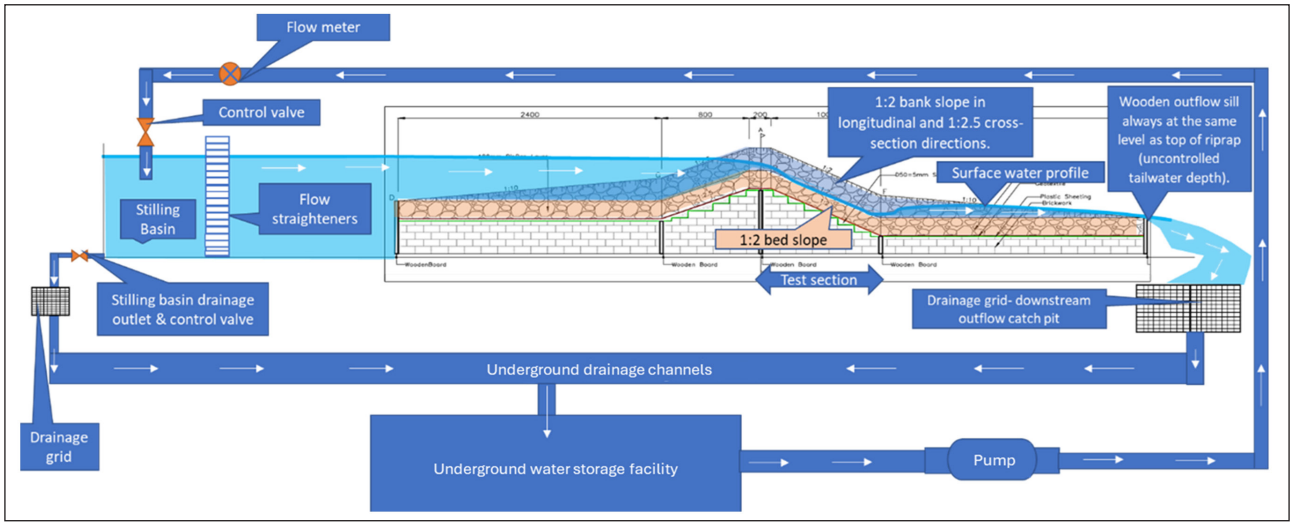

Figure 3. Longitudinal profile of the laboratory setup of the physical hydraulic model (1:2 bed slope)

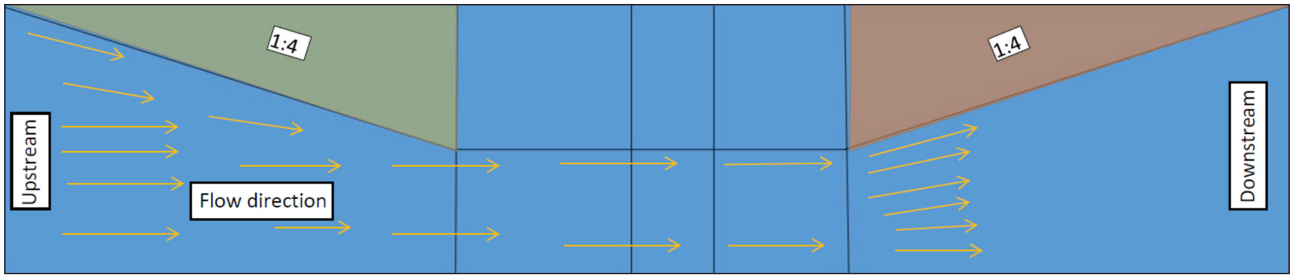

Figure 4. Plan view of physical model showing typical fluid flow lines near the bed

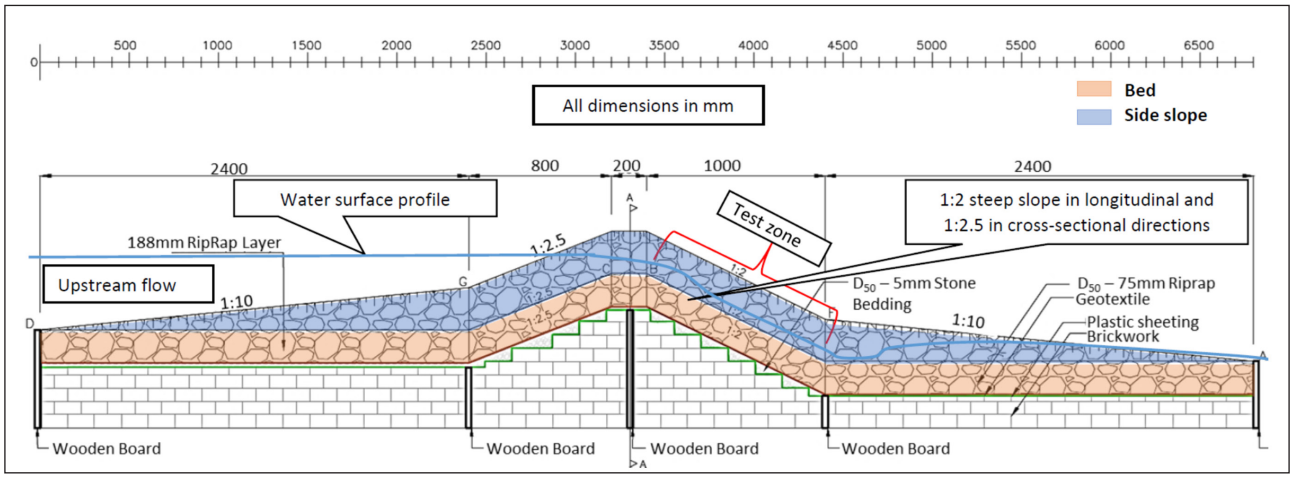

Figure 5. Typical longitudinal cross-section of physical model with a steep 1:2 downstream (chute type) slope in the testing area without tailwater control

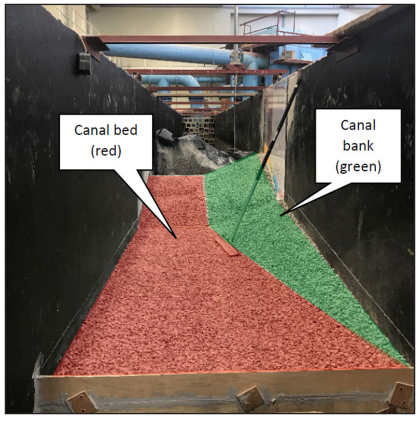

Figure 6. Finished foundation level of the model, viewed from downstream looking upstream

Riprap properties

Riprap shape, material, and density

Angular hornfel quarried rock material sourced from the Western Cape Province of South Africa was used to perform the tests. The density of the hornfel riprap rocks was assumed to be 2 700 kg/m^3 based on the laboratory results of Langmaak and Basson (2015) and design rock density recommendations by CIRIA (2007).

Specific literature determining the drag coefficient (C_D) or the settling velocity of angular riprap rocks could not be found. A similar study by Langmaak and Basson (2015) obtained a drag coefficient of 1.66 for large angular and sub-angular riprap rocks. The C_D is dependent on size, shape, and density, thus Armitage (2002) recommends that the drag coefficient of irregular shapes be physically determined at the laboratory.

To determine the settling velocity of angular riprap, tests were conducted for the three rock size ranges, i.e., 0.026–0.038 m, 0.038–0.053 m, and 0.053–0.075 m. While 120 settling tests were conducted, only 45 tests were successfully executed and measured. Each stone in the three sample ranges was measured for the three dimensions i.e., *a*, *b* and *c*, as defined in the Corey shape factor (Simon and Senturk, 1992) equation as follows:

$$\mathrm{CSF} = \frac{c}{\sqrt{ab}}, \tag{10}$$

with *a* the longest axis dimension of the stone, *b* intermediate axis dimension, and *c* the shortest axis dimension. To experimentally determine the drag coefficient, the settling velocity was used (Graf, 1971; Raudziki, 1998):

$$v_{ss} = \sqrt{\frac{4}{3}\frac{(\rho_r - \rho_w)}{\rho_w}\frac{gD_{50}}{C_D}} \tag{11}$$

The settling velocity (v_{ss}) for each riprap rock in the samples was determined experimentally using the following equation:

$$v_{ss} = \frac{\mathrm{Distance}\left(\mathrm{travelled\ by\ rock\ in\ settling\ tank}\right)}{\mathrm{Time}\left(\mathrm{recorded\ with\ stopwatch}\right)} \tag{12}$$

The density of water and riprap was assumed to be 1 000 and 2 700 kg/m^3, respectively. The intermediate dimension *b* of each rock was considered to be representative of D_{50}. Subsequently, the drag coefficients were calculated from the experimentally measured settling velocities. The results for the drag coefficient versus the respective settling velocities and Corey shape factors are shown in Fig. 7.

From Fig. 7, the average Corey shape factor for the 45 data points was found to be 0.529, and the corresponding C_D using the trendline equation was 2.17. Therefore, the average drag coefficient for angular riprap rock was determined to be 2.17. This value is considered acceptable as it is relatively close to the drag coefficient of 1.66 found in the Langmaak and Basson (2015) study, which also used similar rock shapes. The discrepancy in the drag coefficients of the two studies may be attributed to the irregular nature of riprap rocks. Other factors contributing to the difference could be slight variations in the methods followed by Langmaak (2013) and this study in determining the settling time.

Riprap gradation

The non-uniform grading criterion recommended by Simon and Senturk (1992), as outlined in Eq. 13, was implemented to both the D_{50} = 0.038 m and D_{50} = 0.075 m median stone sizes, resulting in riprap with grading curves as presented in Fig. 8:

$$D_{100} \geq 2D_{50},\ D_{20} \geq 0.5D_{50},\ D_{\min} \geq 0.2D_{50} \tag{13}$$

Riprap angle of repose

Froelich (2011) conducted a study on 74 natural and crushed stockpiles of open-graded quarry rock, leading to the development of a simple regression equation to predict the mass angle of repose:

$$\ln\phi_r = 3.43 + 0.0799I_1 + 0.183I_2 + 0.125\ln\left(\frac{D_{85}}{D_{50}}\right) \tag{14}$$

One advantage of using Eq. 14 is its ability to incorporate the grading of riprap mixtures through the grading length ratio $\left(\frac{D_{85}}{D_{50}}\right)$. This allows the equation to be applicable to different D_{50} stone sizes and grading, as the grading length ratio $\left(\frac{D_{85}}{D_{50}}\right)$ adjusts for these variations.

The angles of repose calculated with Eq. 14 for both the D_{50} = 0.038 m and D_{50} = 0.075 m median stone sizes, as listed in Table 2, were found to be approximately equal. Therefore, a rounded value of 40° for the angle of repose for angular riprap was assumed.

Experimental setup and procedure

A high-resolution video camera was used to capture images for tracking riprap movement in the test zone. Riprap incipient failure flow rates were measured by a Proline PROMAG W and Flowmetrix SAFMAG electromagnetic flowmeter, with measuring errors of ± 0.00017 m^3/s and ± 0.0005 m^3/s, respectively. Additionally, a point gauge needle and a total station setup were used to measure the pertinent bed and water elevations.

The camera and total station were positioned strategically in the laboratory. The physical model was gradually saturated and controlled to remove trapped air inside the model, ensuring only stable riprap rocks remained on the surface of the steep slope in the testing zone. The flow rate was then incrementally increased until the incipient failure of riprap occurred. The camera captured the movement of the riprap on the test zone, while the Leica total station recorded the surface water elevation measurements at incipient failure.

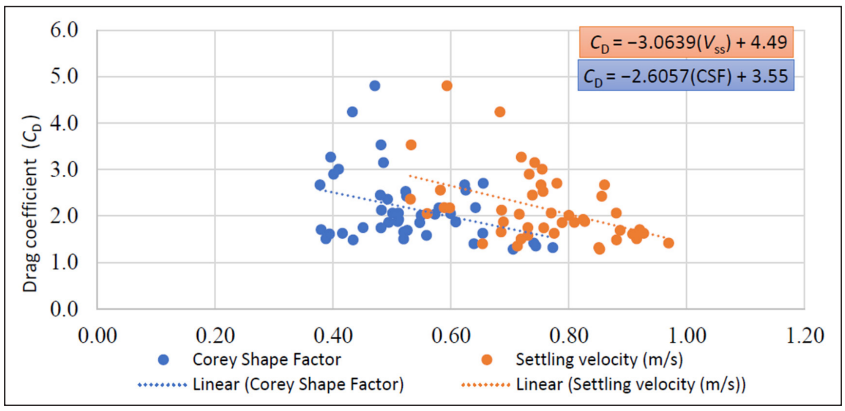

Figure 7. Relationship between Corey shape factor and drag coefficients, as well as settling velocities, for a sample of 45 rocks

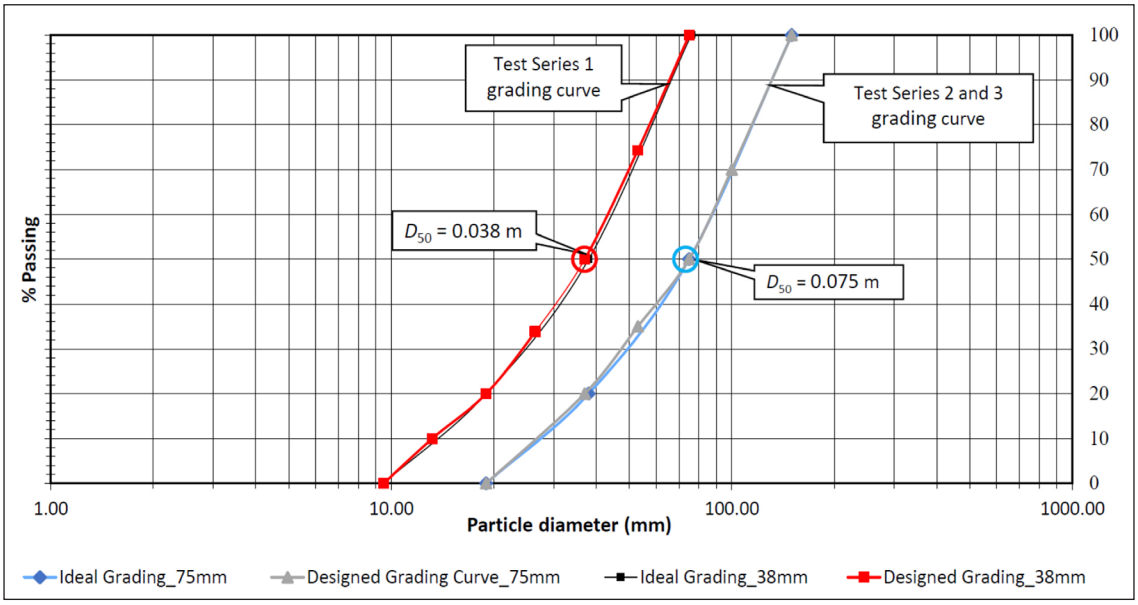

Figure 8. Riprap particle distribution curves for D_{50} = 0.038 m and D_{50} = 0.075 m riprap layer

Table 2. Angle of repose for the two riprap layers

Riprap D_{50} (m)	Riprap D_{85} (m)	Angle of repose φ_r (°)
0.038	0.064	39.6
0.075	0.123	39.4

To conduct an MN analysis, accurate measurements of the water depth, bed slope, side-bank slopes and the angle of repose of the rock are essential. Local average slopes and water depths were physically measured in the laboratory. According to Novak (1999), the water depth on steep bed slopes should be measured perpendicular to the bed slope, denoted as component D_w in Fig. 9. The vertical component D_v was derived from the difference between the bed and water surface elevations. Therefore, D_w was calculated using the following relation:

$$D_w = D_V \cos\theta \tag{15}$$

Golden Surfer version 15 (hereafter referred to as Surfer v15) was used to convert surveyed data into contour elevation data, enabling the retrieval of water depths from the laboratory-measured data as illustrated in Fig. 9. Surface water elevation measurements for incipient failure conditions were identified locally, and the water depth in the local failure region was used for the MN analysis. The encircled area in Fig. 10 and Fig. 11 represents a typical riprap local failure zone in one of the tests.

The local failure zone was identified as an area approximately 0.2 m by 0.2 m in all the tests conducted in the laboratory. The red dots in Fig. 11 indicate where the local average flow depth and average bed slopes were computed for the MN analysis.

In each identified local failure zone for each test, 50 mm incremental profiles (as shown in Fig. 9) were analysed. This approach eliminated bias that may arise if a single longitudinal cross-section (e.g., the red line in Figs 10 and 11) was assumed to provide the relevant water depth in each test scenario. The authors noted variations in water depth due to bed roughness irregularities. Therefore, the measurement method adopted aimed to account for these variations within the local failure zone. Consequently, each test performed a maximum of 20 measurements of average water depth and average bed slope within the identified 0.2 m by 0.2 m failure zone. A probabilistic MN analysis could be performed for each test based on the measured data in each local failure zone.

RESULTS

Approach to analysis

The incipient motion conditions were analysed using Liu's (1957) MN approach. To account for the influence of the steep bed and steep side-bank slopes, the steep bed correction factors recommended by Armitage (2002) were applied. Thus, Eq. 9 was used to calculate the MN for all the tests.

Table 3 summarises all critical input parameters necessary to calculate the MN at incipient failure for all three test series. The settling velocities of the riprap rock were experimentally determined.

The dimensionless particle Reynold number (Re.) was calculated as follows (Cheng, 1997, and Armitage, 2002):

$$\mathrm{Re}_* = \frac{u^* D_{50}}{\nu} \tag{16}$$

where u^* is the shear velocity and ν is the kinematic viscosity of the fluid.

Test Series 1 MN results

Figure 12 shows the characteristic curves by Rooseboom (1992) and Armitage (2002). Armitage's (2002) curve was based on $\mathrm{MN} = \frac{2}{\mathrm{Re}_*}$ for the hydraulic laminar region flow regime ($\mathrm{Re}_* < 11.8$) and MN = 0.17 for turbulent flow regime ($\mathrm{Re}_* > 11.8$). In contrast, Rooseboom's (1992) curve used $\mathrm{MN} = \frac{1.6}{\mathrm{Re}_*}$ in laminar flow ($\mathrm{Re}_* < 13$) and MN = 0.12 for turbulent flow ($\mathrm{Re}_* > 13$).

For Test Series 1, a total of 135 MN values were calculated, with 128 MN data points exceeding the upper limit of 0.17. This indicates that only 5.2% of the data points fell below the 0.17 MN value, suggesting that 94.8% of the MN values were above the critical 0.17 MN value, indicating a predominance of turbulent flow conditions.

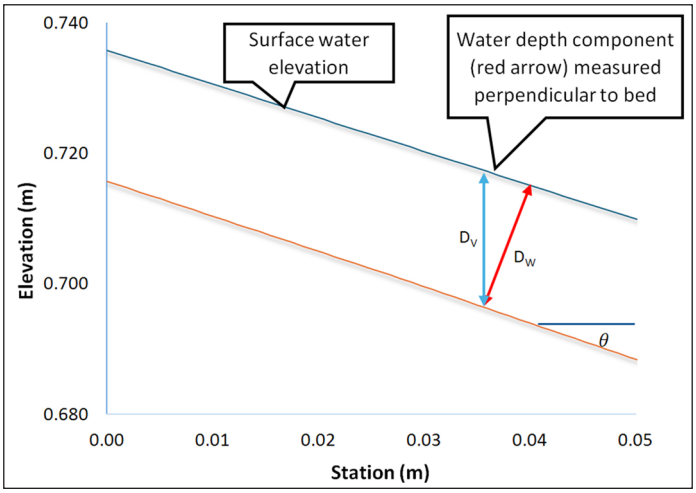

Figure 9. Water depth determination components (elevation and station in m)

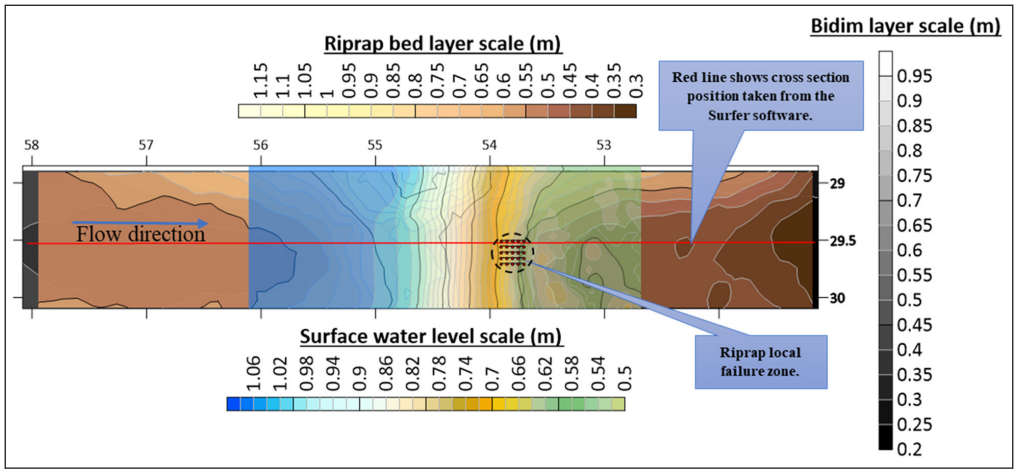

Figure 10. Contour elevation data produced with Surfer v15

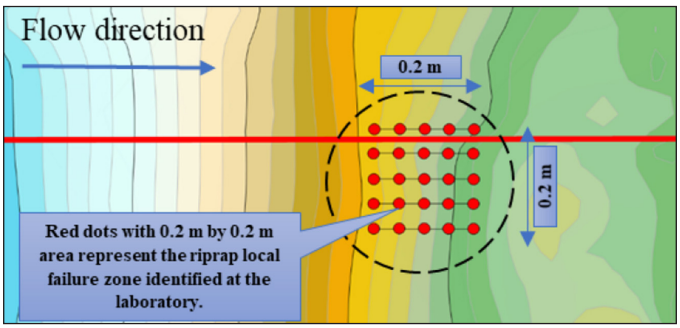

Figure 11. Exaggerated section (extracted from Fig. 9) showing the local failure zone

Table 3. Hydraulic input parameters

Input parameter	Test Series 1	Test Series 2 and 3	Unit
D_{50}	0.038	0.075	M
ρ_r	2 700	2700	kg/m^3
ρ_w	1 000	1000	kg/m^3
v_{ss}	0.6393	0.8352	m/s
$\varphi_{r\ (riprap)}$	40	40	°
$\alpha_{angle\ (side\ slope)}$	21.77	21.77	°
$\alpha_{slope\ (side\ slope)}$	0.4	0.4	
$\theta_{angle\ (bed\ slope)}$	Varied	Varied	°
$\theta_{slope\ (bed\ slope)}$	Varied	Varied	
G	9.81	9.81	m/s^2
D_w	Varied	Varied	m
V	1.13 x 10^{-6}	1.13 x 10^{-6}	m^2/s at 15°C

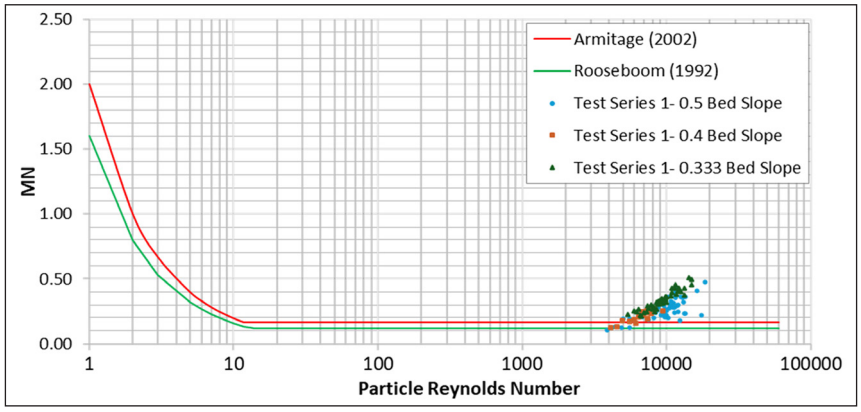

Figure 12. Test Series 1 MN results plotted on the Liu diagram

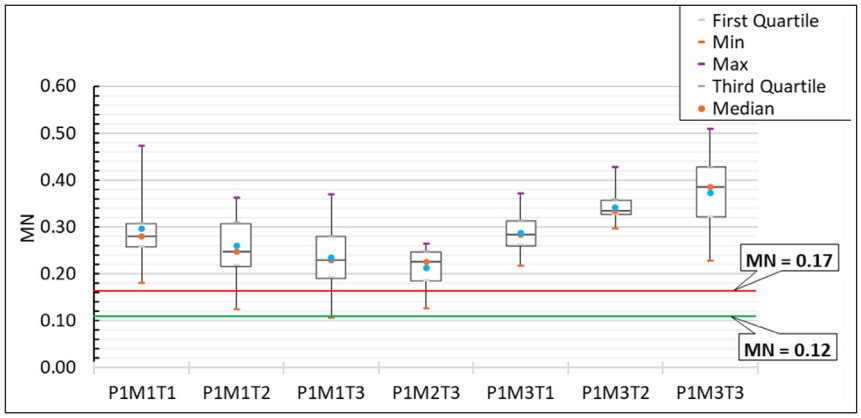

Figure 13. Variation in the MN of the physical laboratory tests in Test Series 1

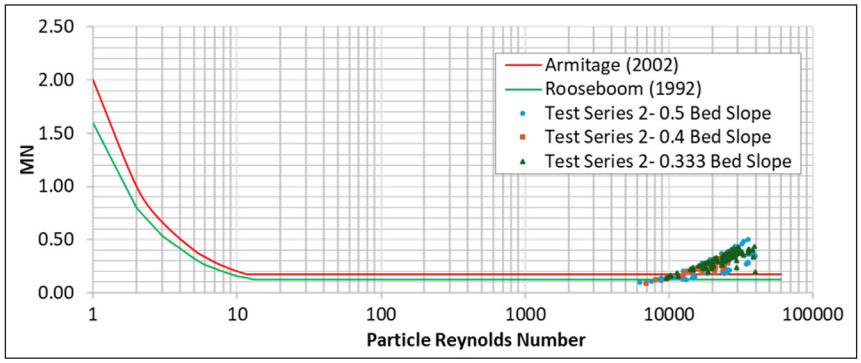

Figure 14. Test Series 2 MN results plotted on the Liu diagram

The scatter of the MN for each test in Test Series 1 was effectively demonstrated using the box-whisker diagram in Fig. 13. The three critical tests, P1M1T2, P1M1T3 and P1M2T3, had the minimum MN values within the 0.12 and the 0.17 MN envelope. An exceedance probability analysis was conducted on these critical MN datasets. The MN of the three critical tests were listed and sorted, with the lowest MN value at the bottom and the highest MN at the top. Subsequently, the 5th percentile was calculated using the Microsoft Excel internal mathematical function; in this context, the 5th percentile represents the 5% probability of exceedance MN value. For Test Series 1, the critical 5% probability of exceedance MN value was determined to be 0.119, which aligns with Rooseboom's (1992) MN value of 0.12.

Test Series 2 MN results

In Fig. 14, a total of 242 out of 264 MN points plotted above the 0.17 upper limit of the envelope, while approximately 8.3% of the total MN values (22 MN) plotted below this limit. The lowest MN value obtained for Test Series 2 was 0.091, as shown in Fig. 14.

To further illustrate the variation in the calculated MN values for each test in Test Series 2, the box-whisker diagram in Fig. 15 was constructed. Tests P2M1T3 and P2M1T4 were excluded from the analysis due to insufficient water depth and slope data measured in the failure region of these two tests, rendering their MN values unreliable.

Tests P2M1T1, P2M2T2, P2M2T4 and P2M3T4 were four reliable tests with the minimum MN values below the 0.17 upper limit MN value. These tests were further analysed using the 5th percentile representing the 5% probability of exceedance. For Test Series 2, the lowest critical MN value with a 5% probability of exceedance was determined to be 0.127. This value closely aligned with the lower limit MN of 0.12 obtained by Rooseboom (1992).

Comparing Test Series 1 and Test Series 2, both followed similar testing procedures and exhibited similar riprap failure behaviour.

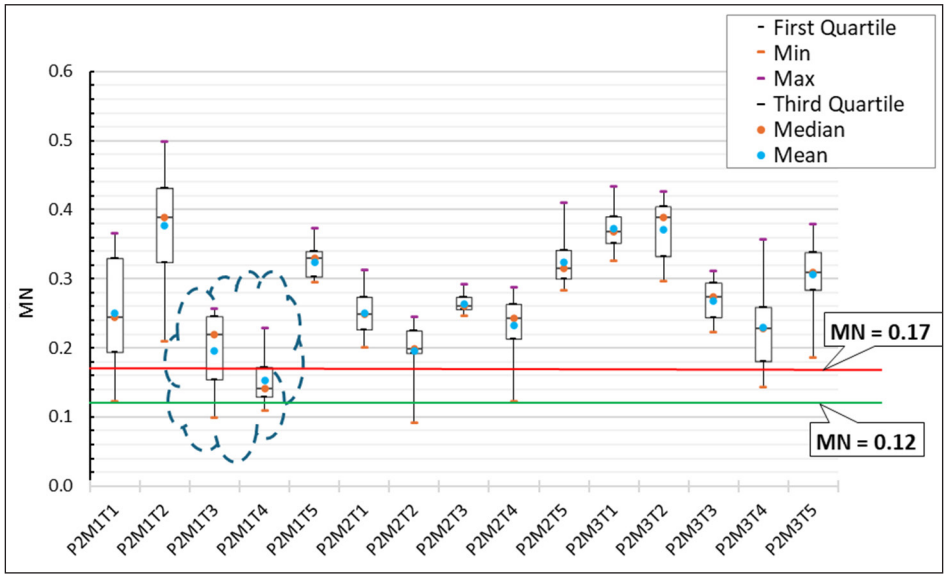

Figure 15. Variation in the MN values of the physical laboratory tests for Test Series 2

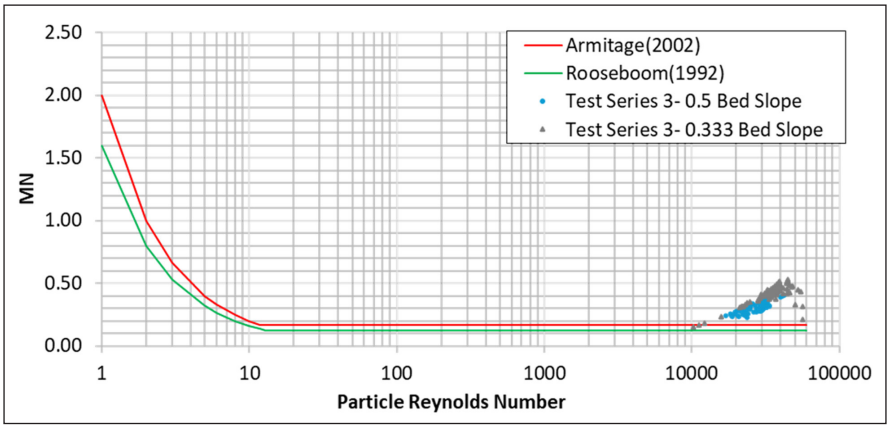

Figure 16. Test Series 3 MN results plotted on the Liu diagram

However, Test Series 1 used a smaller 0.038 m median stone size, while Test Series 2 used a larger of 0.075 m median stone size. It was observed that in both test series, riprap failure occurred only on the steep bed area, with no failure occurring on the side bank due to limited water encroachment on the bank.

The critical incipient failure MN values of 0.119 and 0.127 obtained from the probability of exceedance analysis for Test Series 1 and 2, respectively, yielded satisfactory results. The percentage difference between these two MN values for the critical incipient failure conditions was 6.5%, indicating a high degree of consistency.

Test Series 3 MN results

For Test Series 3, angular riprap dumped in the steep bed area was glued with an adhesive to allow the water to encroach on the side bank, enabling the investigation of incipient failure on the side bank. In Fig. 16, 196 MN values plotted above the 0.12 and 0.17 MN values, while only two MN values plotted below the MN value of 0.17. Most points plotted abundantly from an approximate MN value of 0.22 upwards, aligning with observations made in the laboratory. Higher flow rates and water depths (relative to Test Series 1 and 2) instigated incipient failure of riprap dumped on the 0.4 steep side-bank slope.

Figure 17 shows the box-whisker plot of the MN values of each test in Test Series 3. Model 1 (0.5 bed slope) tests exhibited less variation in the MN values, evident from the compressed nature of the box plots, with all MN values greater than 0.17. However, the Model 3 tests (0.333 bed slope) showed higher MN values compared to Model 1 tests. Test P3M3T1 and P3M3T4 have minimum values below the 0.17 MN value, but these were viewed as potential outliers due to the length of the whiskers in relation to the boxes.

To determine the critical incipient failure conditions, all tests in Test Series 3 were analysed for the 5% probability of exceedance MN value. For Model 1, the lowest 5% percentile MN value was 0.227, while for Model 3, the calculated 5% percentile MN value was 0.181. However, the 0.181 MN value was considered an outlier for several reasons:

- Statistically, all the boxes in Model 3 were positioned further relative to their minimum MN values and box MN values in Model 1 tests
- From the Liu diagram in Fig. 16, only three points had MN values in the 0.12–0.18 range, suggesting that the 0.181 MN value may be an outlier
- The physical model indicated that Model 3's bed slopes showed more resilience in resisting incipient failure, suggesting that the critical MN value must be obtained from Model 1
- Previous research results suggested a critical MN value between 0.12 (Rooseboom, 1992) and 0.17 (Armitage, 2002) or 0.18 (Langmaak and Basson, 2015) for bed slopes, aligning with the expected critical MN value from Model 1's test

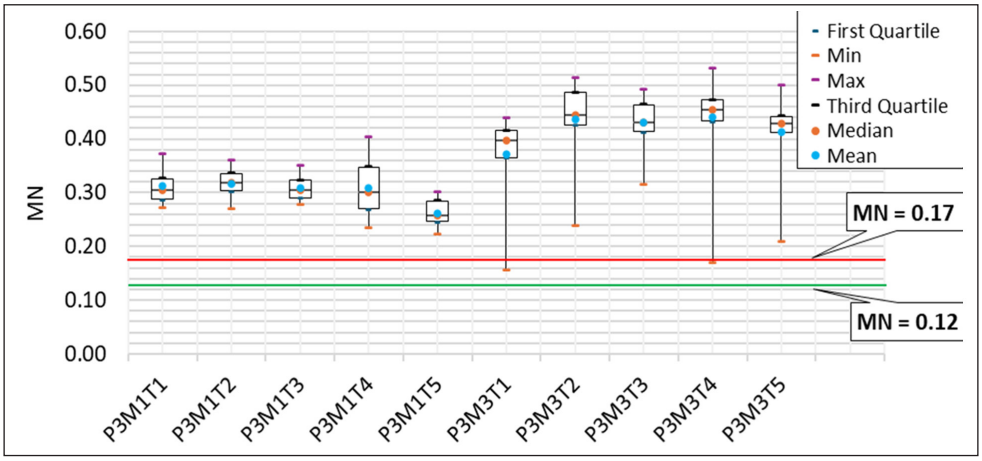

Figure 17. Variation in the MN of the physical laboratory tests for Test Series 3

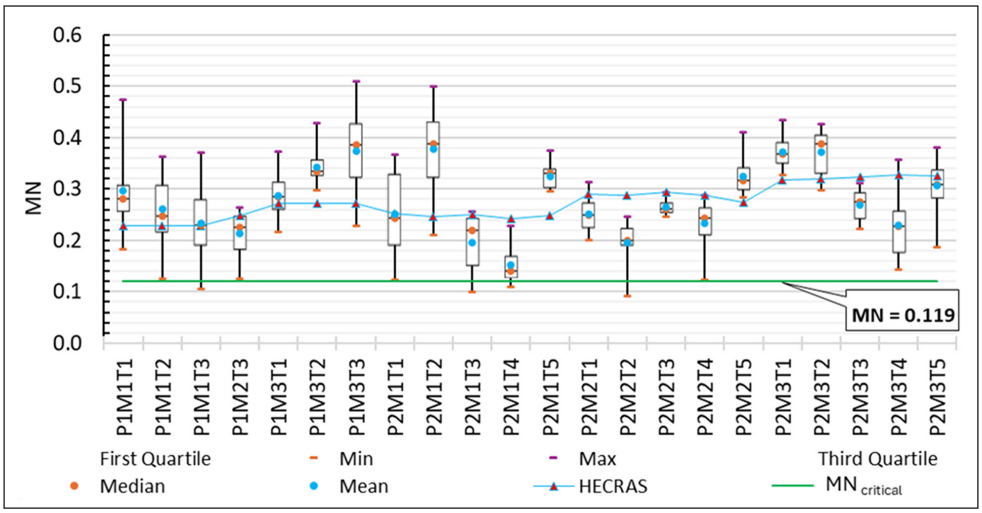

Figure 18. Comparison of experimental and simulated MN values for Test Series 1 and 2

Considering the finding of previous studies and laboratory observations, defining the critical MN value for Test Series 3 as 0.227 from the Model 1 test was more appropriate than the 0.181 MN value from Model 3.

From the above MN analysis, the critical MN value defining the incipient failure conditions of riprap on the steep bed slopes (0.333 to 0.5) was found to be 0.119. The critical MN value defining the incipient failure conditions of angular riprap on steep side banks was found to be 0.227, both determined with a 5% probability of exceedance with respect to the laboratory tests performed.

COMPARISON OF HEC-RAS SIMULATED MN VALUES WITH PHYSICAL MODEL MN RESULTS

The evaluation of the predictive capability of the 1-dimensional HEC-RAS V 5.0.4 software (Hydrologic Engineer Center, 2018) model for determining the physical model's MN values involved conducting steady-state flow analysis to simulate the laboratory tests. The numerical model's geometry was configured to mimic the laboratory setup, with water elevations from the laboratory tests used as boundary conditions. The flow rates for each test were used as input values for the HEC-RAS model simulations. To establish a calibration relative to roughness for the simulations, the Chezy equation was used. Test P2M2T3 served as the basis for calibrating a reliable relative roughness. According to Froelich (2012), the roughness element k_s is defined as:

$$k_s = \alpha_i D_i. \tag{17}$$

For this study, the i is 50 since the incipient failure conditions in this study are related to the D_{50} median riprap rock size. The relative roughness may be represented as follows:

$$\alpha_{50} = \frac{k_s}{D_{50}}. \tag{18}$$

After the calibration the relative roughness α_{50} was found to be 0.316. This allowed for the calculation of the roughness for the same D_{50} median rock size, with k_s being 0.012 for D_{50} of 0.038m and 0.0237 for D_{50} of 0.075 m. The HEC-RAS models were then run using the completed input data, and the average flow depths near the local failure regions were determined. From these simulated average flow depths, along with bed and side-bank slopes, the MN values for HEC-RAS simulated results were determined.

Test Series 1 and 2 HEC-RAS MN values

Figure 18 illustrates the distribution of MN values determined from the HEC-RAS simulations in comparison to those obtained from the physical laboratory tests and the critical MN value of 0.119 derived from the experimental results. Figure 18 shows a range of relationships between the HEC-RAS MN values and the experimental MN values, with some HEC-RAS values falling below, near or above the mean MN values of the physical laboratory tests. Notably, all HEC-RAS MN values exceeded the critical 0.119 critical MN threshold established for Test Series 1 and 2. The HEC-RAS simulations yielded a minimum MN value of 0.227 (from test P1M1T3) and a maximum MN value of 0.391 (from Test P2M3T4). However, no clear trend of correlation was observed between the physical and HEC-RAS MN values.

Test Series 3 HEC-RAS MN values

Figure 19 illustrates that the HEC-RAS simulated MN values for Model 3 consistently fell below the observed MN values in the physical model. The minimum MN value obtained from the HEC-RAS simulations was 0.306, observed in Test P3M1T5, while the highest was 0.391, recorded in Test P3M3T4. Notably, all HEC-RAS MN values exceeded the critical MN value of 0.227 for Test Series 3. For Model 1 of Test Series 3, the HEC-RAS simulated MN results generally plotted above or close to the mean experimental MN values, indicating that HEC-RAS tended to overestimate the MN values.

The comparison and analysis demonstrate that HEC-RAS 1-D software cannot reliably simulate MN results that align with physical model–determined MN values. This discrepancy may be attributed to limitations in the HEC-RAS software's ability to accurately model flow, particularly in scenarios involving porous riprap, rough beds, and complex turbulent and eddy currents.

This evaluation is crucial for engineering design purposes, as some practitioners might rely solely on the MN criteria and HEC-RAS surface water modelling simulation results to determine the appropriate stone size for riprap. Failure to consider the applicable adjustment factors could lead to the specification of an incorrect median stone size for riprap, potentially compromising the stability and effectiveness of the structure.

HEC-RAS MN adjustment factor

Based on the overestimation of the critical incipient failure MN values by HEC-RAS, an adjustment factor (hereafter referred to as AF) was proposed to correct the HEC-RAS simulated MN values. For steep-bed riprap designs, the AF was calculated as the ratio between the lowest MN values from HEC-RAS and the critical MN value obtained from the physical model tests for Test Series 1 and 2 as follows:

$$\mathrm{AF}_{\mathrm{bed}} = \frac{\mathrm{Lowest\,MN}_{\mathrm{HECRAS}}}{\mathrm{MN}_{\mathrm{critical(physical\,model)}}} = \frac{0.227}{0.119} = 1.91 \qquad (19)$$

Similarly, for side-bank riprap design, the AF was calculated as:

$$\mathrm{AF}_{\mathrm{sidebank}} = \frac{\mathrm{Lowest\,MN}_{\mathrm{HECRAS}}}{\mathrm{MN}_{\mathrm{critical(physical\,model)}}} = \frac{0.306}{0.227} = 1.35 \qquad (20)$$

These AF are applicable under specific design conditions:

- HEC-RAS analysis must be performed for 1-dimensional steady-state flow conditions
- The relative roughness applied must be $\alpha_{50} = \frac{k_s}{D_{50}} = 0.316$
- The MN criteria are only applicable to steep bed slopes of 0.5 to 0.333
- The steep side-bank slope must be designed to be 0.4
- The bottom trapezoidal canal width must adhere to the ratio $w_{\mathrm{ratio}} = \frac{\mathrm{Bottom\,width}}{D_{50}} = \frac{1.2\,\mathrm{m}}{0.075\,\mathrm{m}} = 16$ (up to 31 for the D_{50} = 0.038 m median stone size).

Applying these AFs and design conditions listed above ensures that engineers can determine a safe MN value to specify a suitable D_{50} median stone for the design flow rates using HEC-RAS.

GUIDELINES FOR RIPRAP DESIGN IN STEEP BED SLOPES AND SIDE BANKS

The following guidelines are intended to assist designers in specifying stable riprap D_{50} for specific design flow rates on steep bed slopes and steep side banks using HEC-RAS 1-D modelling software. The steps to follow in the design of stable riprap on steep canal bed slopes are:

Step 1: Calculate the settling velocity: Use Eq. 11 to calculate the settling velocity of the riprap. Table 4 provides the required material property inputs, which are based on recommended assumptions for riprap designs (CIRIA, 2007). The D_{50} size should be estimated iteratively, with a reasonable initial D_{50} size to be guessed. The recommended C_D value for design purposes is based on the average C_D value determined in the laboratory. While the

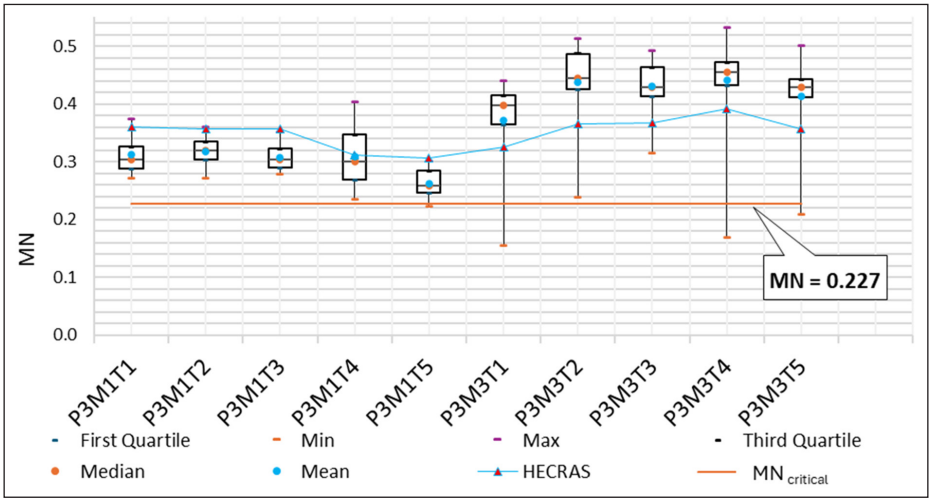

Figure 19. Comparison of experimental and simulated MN values for Test Series 3

Table 4. Properties required to calculate the settling velocity of D_{50}

Water density	ρ_w	1 000	kg/m³
Riprap rock density	p_r	2 700	kg/m³
Gravity acceleration	g	9.81	m/s²
Median rock diameter	D_{50}	0.112	M
Drag coefficient	C_D	2.17	(This is a recommended drag coefficient value.) A smaller drag coefficient may lead to undersized D_{50} specification

designer may select their own C_D, decreasing it from 2.17 may result in an undersized D_{50}, which is not recommended.

Step 2: Determine the steep bed slope correction factor: The design bed slope and angle of repose of the riprap must be known to calculate the steep bed correction factor (Eqs 19 and 20). For angular riprap, a recommended angle of repose of 40° can be used. Alternatively, the designer may determine an angle of repose using a reliable source from the literature.

Step 3: Determine stable D_{50} median stone size: Determine the stone size by using HEC-RAS 1-D steady-state flow analysis to obtain the flow depth. For a specific design flow rate and geometry of the channel, HEC-RAS can compute the respective flow depth on the steep bed slope. The adjustment factor (AF_{bed}) of 1.91 must be applied to the HEC-RAS MN values. Iteratively adjust the initially estimated D_{50} size until the MN value reaches 0.12, which accounts for the critical MN value of 0.119 for steep bed slopes, rounded up to 0.12 to meet design specifications.

The same procedure as above is followed for designing stable riprap on the steep side banks of trapezoidal canal cross-sections, but the side-bank slope correction factor ($AF_{sidebank}$) is included in Step 2. Use Eq. 8 to calculate the $AF_{sidebank}$. Apply the correction factor for the side banks of 1.35 and use the critical MN value of 0.227 for side-bank riprap designs.

The following guidelines can be used for the iterative process of determining the median stone size to achieve the required MN:

- If MN > 0.12 for bed slopes or MN > 0.227 for side banks, increase the D_{50} size.
- If MN = 0.12 for bed slopes or MN = 0.227 for side banks, the design is considered safe.
- If MN < 0.12 for bed slopes or MN < 0.227 for side banks, decrease D_{50} size until MN = 0.12 (bed slopes) or MN = 0.227 (side banks).

The designer should be aware that adjusting the D_{50} will also affect the k_s value. Thus, it is necessary to iterate the process from Step 1 until the water depth, k_s, and D_{50} converge. When these three parameters no longer change after running a HEC-RAS simulation, the converged D_{50} can be recommended as the safe steep-bed design D_{50} for the specific design flow rate. It is, however, recommended that a minimum safety factor of 10% be applied to the calculated D_{50}.

CONCLUSIONS

The study successfully achieved its objectives by conducting physical modelling and analysing the results using MN criteria to determine the critical incipient failure conditions for angular riprap rocks on steep bed slopes and steep side-bank slopes.

The critical incipient failure MN value for angular riprap on wide steep-bed slopes (0.333–0.5) was determined to be 0.119 with a 95% probability of exceedance, consistent with Rooseboom's (2002) criteria defining the critical 0.12 MN value for particles in the turbulent flow regions. Similarly, for steep side slopes (0.4), the incipient failure MN value for angular riprap was found to be 0.227 with a 95% probability of exceedance.

The steady state flow analysis with HEC-RAS 1-dimensional modelling software for riprap in steep bed slopes and steep side-bank slopes tended to overestimate critical MN values compared to the physical model results. Consequently, an adjustment factor (AF) of 1.91 must be applied to the HEC-RAS MN analysis for riprap on steep beds, and an AF of 1.35 for riprap on a steep side-bank slope of 0.4.

The applicability of these findings is limited to riprap in straight trapezoidal cross-sectional channels with steep beds ranging from 0.333 to 0.5 and with side-bank slopes of 0.4. The model D_{50} sizes were 0.038 m and 0.075 m, corresponding to prototype stone sizes with D_{50} between 0.57 m and 1.125 m, respectively. Therefore, the results are only valid for designing a prototype D_{50} stone size within this range, in which the bed bottom width to D_{50} ratio needs to be between 16 and 31.

ACKNOWLEDGEMENTS

This research was conducted at the Civil Engineering Department at Stellenbosch University, South Africa.

NOTATION

a, b and c	Longest, intermediate, and shortest axes of the rock, respectively
AF	Adjustment factor
C_D	Drag coefficient
CSF	Corey shape factor
D_{50}	Median riprap diameter
D_w	Flow depth measured perpendicular to bed
D_v (or y)	Flow depth measured vertically
G	Gravitational acceleration
k_α	Steep side bank correction factor
k_β	Steep bed correction factor
k_s	Roughness of channel
L_{arr}	Arrestor length
MN	Movability number
Re_*	Particle Reynolds number
S_o or θ	Longitudinal bed slope
u^*	Shear velocity
W_{base}	Canal bottom width
A	Side bank angle
B	Steep bed angle
ρ_r	Density of rock
ρ_w	Density of water
τ_0	Bed shear stress
v_{SS}	Settling velocity of riprap
V	Kinematic viscosity
φ_r	Riprap rock angle of repose (40°)

REFERENCES

ARMITAGE N (2002) A unit stream power model for the prediction of local scour. PhD dissertation, Stellenbosch University.

ARMITAGE N and MCGAHEY C (2003) A unit stream power model for the prediction of local scour in rivers. WRC Report No. 1098/1/03. Water Research Commission, Pretoria.

ARMITAGE N and ROOSEBOOM A (2010) The link between movability number and incipient motion in river sediments. *Water SA* **36** (1) 89–96. https://doi.org/10.4314/wsa.v36i1.50911

BLODGETT JC (1986) Rock riprap design for protection of stream channels near highway structures: Volume 2 – Evaluation of riprap design procedures. US Geological Survey, California.

BOSMAN E and BASSON GR (2012) Investigation of unsteady flow conditions at the bottom outlet works due to air entrainment during gate closure:physical modelling. WRC Report No. TT528-12. Water Research Commision, Pretoria.

CHIEW Y-M and PARKER G (1994) Incipient sediment motion on non-horizontal slopes. *J. Hydraul. Res.* **32** (5) 649–660. https://doi.org/10.1080/00221689409498706

CIRIA, CUR and CETMEF (2007) The Rock Manual. *The Use of Rock in Hydraulic Engineering* (2nd edn). C683. CIRIA, London.
COMMITTEE OF STATE ROAD AUTHORITIES (1994) *Guidelines for the Hydraulic Design and Maintenance of River Crossings*. Volume 3. Department of Transport, Pretoria.
DE ALMEIDA GAM and MARTÍN-VIDE JP (2009) Riprap stability: transverse and longitudinal versus continuous protections. *J. Hydraul. Eng.* **135** (6) 447–456. https://doi.org/10.1061/(ASCE)HY.1943-7900.0000031
FERGUSON RI (2005) Estimating critical stream power for bedload transport calculations in gravel-bed rivers. *Geomorphology* **70** (1–2) 33–41. https://doi.org/10.1016/j.geomorph.2005.03.009
GRAF WH (1971) *Hydraulics of Sediment Transport*. McGraw Hill.
GRASS AJ (1970) Initial instability of fine bed sand. *J. Hydraul. Div.* **96** (3). https://doi.org/10.1061/JYCEAJ.0002369
FRIZELL KH, RUFF JF and MISHRA S (1998) Simplified design guidelines for riprap subjected to overtopping flow. *Proc. Annual Association of State Dam Safety Officials (ASDSO) Conf.*, Las Vegas.
FROEHLICH DC (2011) Mass angle of repose of open-graded rock riprap. *J. Irrig. Drainage Eng.* **50** (July) 454–461. https://doi.org/10.1061/(ASCE)IR.1943-4774.0000316
FROEHLICH DC (2012) The rap on river banks: Protecting river banks with loose rock riprap. *Proc. River Flow 2012. 6th International Conference on Fluvial Hydraulics*, 5–7 September 2012, San Jose, Costa Rica. 5–7.
HENDERSON FM (1966) *Open Channel Flow*. Macmillan, New York. 419 pp.
HELLER V (2011) Scale effects in physical hydraulic engineering models. *J. Hydraul. Res.* **49** 293–306. https://doi.org/10.1080/00221686.2011.578914
HYDROLOGIC ENGINEERING CENTER (HEC) (2018) HEC-RAS River Analysis System computer software. U.S. Army Corps of Engineers, Davis, CA.
LANGMAAK KR (2013) Incipient motion of riprap on steep slopes. Master's thesis, University of Stellenbosch.
LANGMAAK KR and BASSON GR (2015) Incipient motion of riprap on steep slopes. *J. Hydraul. Eng.* **141** (9) 0601510:1-7. https://doi.org/10.1061/(ASCE)HY.1943-7900.0001016
LIU HK (1957) Mechanics of sediment-ripple formation. *J. Hydraul. Div.* **83** (2). https://doi.org/10.1061/JYCEAJ.0000075
MAYNORD ST, RUFF JF and ABT SR (1989) Riprap design. *J. Hydraul. Eng.* **115** (7) 937–949. https://doi.org/10.1061/(ASCE)0733-9429(1989)115:7(937)
NOVAK P (1999) Discussion of "Roughness of loose rock riprap on steep slopes" by CE Rice, KC Kadavy and KM Robinson'. *J. Hydraul. Eng.* **124** (2) 179–185. https://doi.org/10.1061/(ASCE)0733-9429(1998)124:2(179)
RAUDZIKI AJ (1998) *Loose Boundary Hydraulics*. A. A. Balkema, Rotterdam.
ROOSEBOOM A (1974) Open channel fluid mechanics. Tech. Report no. 62. Dept Water Affairs, Pretoria.
ROOSEBOOM A (1992) *Sediment Transport in Rivers and Reservoirs – A Southern African Perspective*. Report No. 297/1/92. Water Research Commission, Pretoria.
ROOSEBOOM A and MULKE FJ (1982) Erosion initiation. *Recent Developments in the Explanation and Prediction of Erosion and Sediment Yield (Proceedings of the Exeter Symposium, July 1982.* 59–66.
SADAT-HELBAR SM, AMIRI-TOKALDANY E, DARBY S and SHAFAIE A (2009) Fall velocity of sediment particles. *Proc. 4th International Conference on Water Resources and Hydrology*, February 2009, Cambridge.
SIMONS DB and ŞENTÜRK F (1992) *Sediment Transport Technology: Water and Sediment Dynamics*. Water Resources Publications, Littleton, Colo.
SHIELDS A (1936) Anwendung der Aehnlichkeitsmechanik und Turbulenzforschung auf die Geschiebebewegung. Mitteil. Preuss. Versuchsanst. Wasser, Erd, Schiffsbau, Berlin no. 26.
STEVENS MA, SIMONS DB and RICHARDSON EV (1979) Hydraulic design of stable channels in alluvial materials. U.S. Army Corps of Engineers, Waterways Experiment Station, Vicksburg, Mississippi.
YANG CT (1972) Unit stream power and sediment transport. *J. Hydraul. Div.* **98** (10). https://doi.org/10.1061/JYCEAJ.000343
YANG CT (1973) Incipient motion and sediment transport. *J. Hydraul. Div.* **99** (10) 1679–1703. https://doi.org/10.1061/JYCEAJ.0003766
YANG CT and STALL JB (1974) Unit stream power for sediment transport in natural rivers. Illinois University Water Resources Centre Research Report. Illinois University, Urbana, IL.
YANG CT (1984) Unit Stream Power Equation for Gravel. *J. Hydraul. Eng.* **110** (12) 1783–1797. https://doi.org/10.1061/(ASCE)0733-9429(1984)110:12(1783)